Multiscale Simulation Framework for Coupled Fluid Flow and Mechanical Deformation

DOE Award: DE-FG02-06ER25726
Final Report

Principal Investigator: Prof. Hamdi Tchelepi

1 Introduction

Numerical simulation of multiphase flow in large-scale heterogeneous reservoirs is computationally demanding. To reduce the computational complexity of obtaining high-resolution solutions, several MultiScale (MS) methods have been developed [1, 2, 3, 4, 5, 6, 7, 8, 9]. In MS methods, the global discrete fine-scale problem is decomposed into local problems using a superimposed coarse grid. Basis functions, which are numerical solutions of local problems, are used to construct accurate coarse-scale quantities. Once the coarse-scale system is solved, the solution is mapped onto the fine scale using the basis functions. Among the existing multiscale methods, the MultiScale Finite Volume (MSFV) [6] formulation provides locally mass-conservative solutions, which is a crucial property for solving coupled flow and transport problems, at a relatively small cost.

The MSFV method employs locally computed basis functions to construct the coarse-scale system in a finite-volume framework. To obtain a locally conservative velocity field at the fine scale, additional local Neumann problems are defined and solved for the primal-coarse control volumes. Recent MSFV developments include incorporating the effects of compressibility [10, 11], gravity and capillary [12], complex wells [13, 14], faults [15], fractures [16], three-phase [17] and compositional displacements [18]. Furthermore, the efficiency of the method has been enhanced by adaptive computation of the basis functions for time-dependent, multiphase displacement problems [19, 20, 21, 22].

For a wide range of heterogeneous problems, the MSFV results have been shown to be in good agreement with reference fine-scale solutions. However, the accuracy of MSFV method suffers from the presence of extreme permeability contrasts (e.g., SPE 10 bottom section [23]), or highly anisotropic problems (e.g., large grid aspect ratios) [24]. To overcome these difficulties, the iterative MSFV (i-MSFV) method was introduced [25], where the MSFV errors are reduced with the help of locally computed Correction Functions (CF). The convergence rate was improved significantly by using the MSFE operator (i-MSFE) [26]. The benefit of the MSFV operator is that a mass-conservative solution is obtained. Thus, the MSFV reconstruction step can be employed at the end of the iterative process to ensure that the approximate numerical solution is mass conservative.

Both the original (single-pass) and iterative multiscale methods can be formulated in an algebraic manner [11, 26]. The algebraic formulation reduces the implementation complexity, especially for problems defined on unstructured grids, and it allows for easy integration of the method into existing reservoir simulators. The Two-Stage Algebraic Multiscale Solver

(TAMS) [26] consists of local and global stages. In the global stage, low frequency errors are resolved by a multiscale preconditioner. In the local stage, high frequency errors are resolved using Block ILU with zero fill-in (BILU) [27]. However, CF was not incorporated into TAMS, and the exact role of CF in the context of multi-stage preconditioning had not been analyzed. In addition, the best choices among the variety of possible local and global stages have not been thoroughly investigated.

In this work, a general iterative Algebraic Multiscale Solver (AMS) is described. AMS allows for MSFV, or MSFE, as global operators with different types of local boundary conditions, and it allows for many local fine-scale solvers. We show that the Correction Functions (CF) can be seen as an independent local preconditioning stage aimed at resolving high-frequency errors. The effects of the CF local stage on the convergence rate and the overall computational efficiency of AMS are analyzed for several heterogeneous problems. To obtain the best combination of methods/stages, we report on performance results considering different global (MSFV, MSFE) and local (BILU, CF, ILU) stages with different local boundary conditions. We then compare the computational efficiency of AMS with that of a state-of-the-art Algebraic MultiGrid (AMG) solver [28].

2 Algebraic Multiscale Solver (AMS)

The pressure equation for incompressible fluid flow in a heterogeneous reservoir can be written as

$$\nabla \cdot (\boldsymbol{\lambda} \cdot \nabla p) = \nabla \cdot (\rho g \boldsymbol{\lambda} \cdot \nabla z) + \tilde{q}, \tag{1}$$

where $\boldsymbol{\lambda}$ is the positive-definite mobility tensor, $\tilde{q}$ represents source terms, g is the gravitational acceleration acting in the ∇z direction, and ρ is the density.

The MSFV method employs two overlapping coarse grids referred to as primal- and dual-coarse grids, which are superimposed on the given fine grid (Fig. 1). There are N_C primal-coarse cells (control volumes), Ω_i^C ($i \in \{1, \cdots, N_C\}$), and N_D dual-coarse cells (local domains), Ω_j^D ($j \in \{1, \cdots, N_D\}$).

Equation (1) discretized on the fine grid, can be written as

$$Ap = q. \tag{2}$$

For Two-Dimensional (2D) problems on structured grids, the dual-coarse grid divides the fine cells into three categories: interior (white), edge (blue), and vertex (red) cells, as illustrated in Fig. 2 [29, 30]. The vertices serve

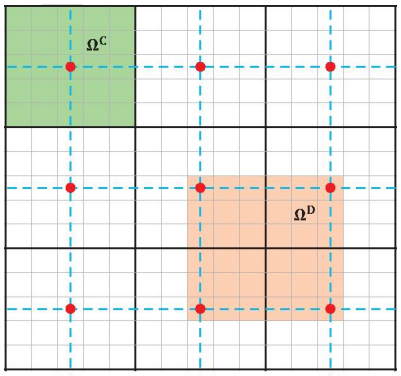

Figure 1: Primal (bold black) and dual (dashed blue) coarse cells. Fine cells belonging to a coarse cell (control volume) are shown in green. Fine cells that belong to a dual-coarse cell are shown in light orange. The red circles denote the coarse nodes (vertices).

as the coarse-grid nodes, and the edge cells denote the boundaries of the dual-coarse cells. For Three-Dimensional (3D) problems on structured grids, an additional category is 'face' cells. Finally, internal cells are those that lie inside dual-coarse cells.

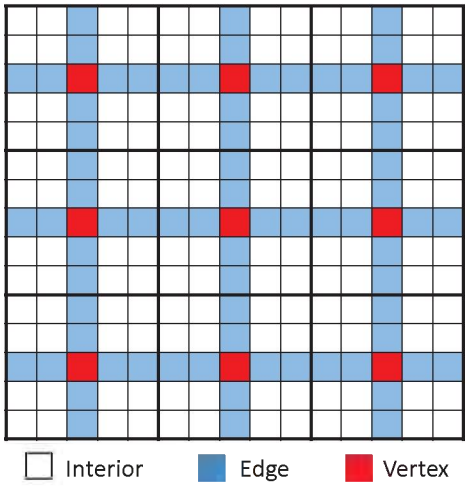

Figure 2: Ordering of the fine cells based on the imposed dual-coarse grid. Also shown with bold solid lines is the primal coarse grid.

A wirebasket reordered fine-scale system [30] can be expressed as

$$\begin{bmatrix} A_{II} & A_{IE} & 0 \\ A_{EI} & A_{EE} & A_{EV} \\ 0 & A_{VE} & A_{VV} \end{bmatrix} \begin{bmatrix} p_I \\ p_E \\ p_V \end{bmatrix} = \begin{bmatrix} q_I \\ q_E \\ q_V \end{bmatrix}, \tag{3}$$

where a local matrix A_{ij} represents the contribution of cell j to the discrete mass-conservation equation of cell i.

The multiscale (approximate) solution can be expressed algebraically as follows:

$$p' = \mathcal{P} p'_V + \mathcal{C} q, \tag{4}$$

where $\mathcal{P}$ and $\mathcal{C}$ are referred to as 'prolongation' and 'correction' operators [31, 32]. To compute p'_V, the following coarse-scale system is constructed and solved

$$A_C p'_V = R_C. \tag{5}$$

Here,

$$A_C = \mathcal{R} A \mathcal{P}, \tag{6}$$

and

$$R_C = \mathcal{R} q - \mathcal{R} A \mathcal{C} q. \tag{7}$$

The restriction operator, $\mathcal{R}$, is $N_C \times N_F$, where N_F is the number of fine-scale cells, and can be based on finite-volume, or finite-element, schemes. For the standard finite-volume operator, the fine-scale equations in a coarse cell are simply summed up, so that $\mathcal{R}$ can be written as:

$$\mathcal{R}(i,j) = \begin{cases} 1 & \text{if } \Omega_j^F \subset \Omega_i^C \\ 0 & \text{otherwise} \end{cases} \quad \forall i \in \{1, \ldots, N_C\}; \forall j \in \{1, \ldots, N_F\}\,. \tag{8}$$

The condition $\Omega_j^F \subset \Omega_i^C$ is true, if the fine cell j (Ω_j^F) belongs to the coarse control volume i (Ω_i^C). The finite-element based restriction operator is the transpose of the prolongation operator, i.e.,

$$\mathcal{R} = \mathcal{P}^T. \tag{9}$$

With the prolongation and restriction operators fully specified, one can solve the coarse-scale system (MSFV, or MSFE) for p'_V. Then, Eq. (4) is used to prolong the coarse-scale solution onto the fine scale, i.e.,

$$p \approx p' = \Big[\mathcal{P}(\mathcal{R}A\mathcal{P})^{-1}\mathcal{R}(I - A\mathcal{C}) + \mathcal{C}\Big] q. \tag{10}$$

Finally, one can define the multiscale (MS) preconditioner with CF (which is referred to as MSWC) as

$$M_{mswc}^{-1} = \mathcal{P}(\mathcal{R}A\mathcal{P})^{-1}\mathcal{R}(I - A\mathcal{C}) + \mathcal{C}. \tag{11}$$

Equation (11) can be rewritten as

$$\begin{aligned} M_{mswc}^{-1} &= \mathcal{P}(\mathcal{R}A\mathcal{P})^{-1}\mathcal{R} + \mathcal{C} - \mathcal{P}(\mathcal{R}A\mathcal{P})^{-1}\mathcal{R}A\mathcal{C} \\ &= M_{ms}^{-1} + \mathcal{C} - M_{ms}^{-1}A\mathcal{C}. \end{aligned} \tag{12}$$

In other words, the iterative procedure

$$p^{\nu+1} = p^{\nu} + M_{mswc}^{-1}(q - Ap^{\nu}) \tag{13}$$

is equivalent to the following two-stage iterative scheme

$$p^{\nu+1/2} = p^{\nu} + \mathcal{C}(q - Ap^{\nu}) \tag{14}$$

$$p^{\nu+1} = p^{\nu+1/2} + M_{ms}^{-1}(q - Ap^{\nu+1/2}). \tag{15}$$

The two steps are: (1) update the solution with the CF operator; (2) update with the multiscale preconditioner $M_{ms}^{-1} = \mathcal{P}(\mathcal{R}A\mathcal{P})^{-1}\mathcal{R}$, which does not involve CF. Therefore, the operator $\mathcal{C}$ is a totally independent stage. This helps to quantify the impact of CF on the iterative multiscale solution strategy. Thus, a general way of writing the AMS-based multi-stage strategy is:

$$p^{\nu+1/2} = p^{\nu} + M_{local}^{-1}(q - Ap^{\nu}) \tag{16}$$

$$p^{\nu+1} = p^{\nu+1/2} + M_{ms}^{-1}(q - Ap^{\nu+1/2}). \tag{17}$$

where M_{local}^{-1} is any local-stage preconditioner, such as ILU, BILU, and CF, and M_{ms}^{-1} is the MS preconditioner used for the global stage. For the MS step, different restriction schemes (e.g., Finite Volume (FV), or Finite Element (FE)) may be used, as will as different local boundary conditions (reduced, or linear, boundary conditions) to construct the MS operator. Next, we study the behaviors of various AMS linear-solver strategies, and we report on the best overall combination.

3 Numerical Results

In this section, systematic tests are performed to find the best combination of local and global stages. For the following experiments, five sets of log-normally distributed permeability fields with spherical variograms are generated using sequential Gaussian simulations [33]. For all the test cases, the variance and mean of $ln(k)$ are 4 and -1, respectively. The fine-scale grid size and dimensionless correlation lengths in the x, y, and z direction (i.e., ψ_x, ψ_y and ψ_z) are shown in Table 1. Each set has 20 equiprobable realizations. For sets 1 and 2, 20 realizations with different orientation angles (Fig. 3) of

0, 15, 30, and 45 degrees are considered. For sets 3 ,4 and 5, 20 realizations of patchy domains are used (Fig. 4). The pressure is fixed on the left and right faces with dimensionless values of 1 and 0, respectively. GMRES preconditioned by the AMS is employed, and iterations are performed until a reduction of five orders of magnitude in the relative l^2 norm of the residual (i.e., $\|r_k\|_2/\|r_0\|_2 \leq 10^{-5}$) is achieved.

Permeability set	1	2	3	4	5
Fine-scale grid	128^3	64^3	128^3	64^3	32^3
ψ_x	0.5	0.5	0.125	0.125	0.125
ψ_y	0.03	0.03	0.125	0.125	0.125
ψ_z	0.06	0.01	0.125	0.125	0.125
Angle between ψ_x and y direction	0°, 15°, 30°, 45°		patchy		
Variance	4				
Mean	-1				

Table 1: Five permeability sets (each with 20 equiprobable realizations) are used for the numerical experiments. Layered fields, i.e., sets 1 and 2, are generated for four different inclination angles, each of which has 20 equiprobable realizations.

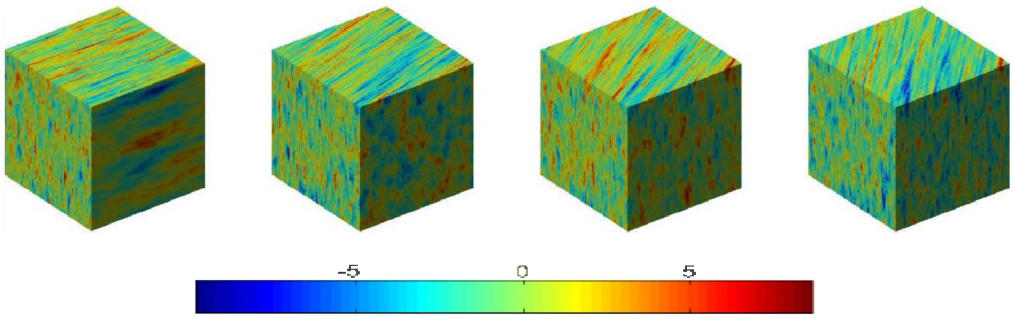

Figure 3: Natural logarithm of one realization of permeability set 1 with angles of 0°, 15°, 30° and 45° from left to right. For each angle, 20 realizations are considered.

3.1 AMS Global Stage: MSFV versus MSFE

The performance of the two different restriction schemes, namely MSFV and MSFE, is investigated using permeability sets 1 and 3. The fine and coarse

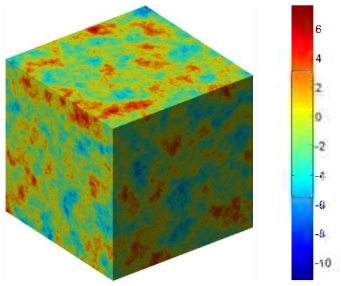

Figure 4: Natural logarithm of one (out of 20 statistically-the-same) realization of the permeability set 3.

grids contain $128 \times 128 \times 128$ and $16 \times 16 \times 16$ cells, respectively. ILU is employed as the sole local preconditioner. As Fig. 5 shows, the FE coarse-scale operator outperforms the FV one for both permeability sets.

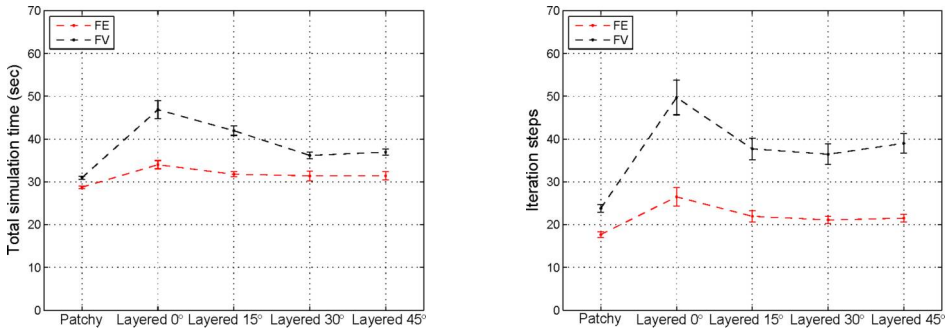

(a) (b)

Figure 5: Comparison of (a) total simulation time and (b) iteration steps for FE and FV global solvers (i.e., restriction operator) on layered and patchy permeability fields over 20 different realizations. Also shown in error bars are the standard deviations. Clearly, FE restriction operator outperforms the FV one.

3.2 AMS Global Stage: Local Boundary Conditions

The effects of different local boundary conditions (BC), i.e., reduced BC and linear BC, are studied here. Permeability sets 2 and 4 are used for

this purpose. The coarse-grid size is $8 \times 8 \times 8$, and ILU is employed as the local preconditioner. Fig. 6 shows that for 'patchy' domains, the reduced and linear BC have similar performance. For layered permeability fields, however, the linear BC improves the computational efficiency of MSFV. Nevertheless, MSFV with linear BC is still not competitive with MSFE.

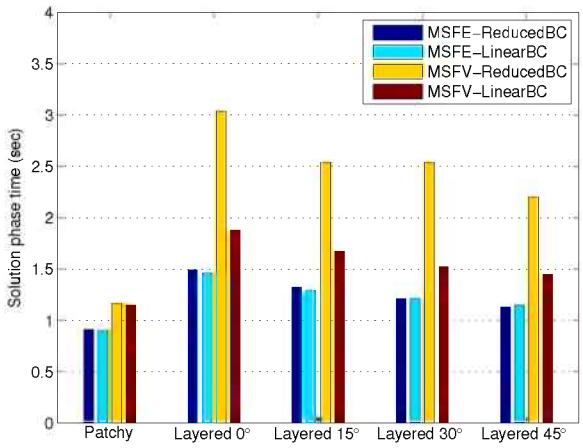

Figure 6: Solution phase time (i.e. excluding setup time) averaged over 20 equiprobable realizations for MSFV and MSFE restriction schemes with linear and reduced boundary conditions.

3.3 AMS Local Stage

Overall, MSFE with the reduced-boundary condition is found to be the most efficient global-stage solver. Next, we investigate which local stage preconditioner is the best overall choice. BILU is used as the second stage preconditioner in TAMS [26]. Here, ILU is employed as the local preconditioner. Based on our experiments, the solution time of BILU and ILU are comparable; however, ILU has minimal setup time compared with BILU. Hence, overall, ILU outperforms BILU in terms of computational time. A comparison between ILU and BILU is performed for permeability sets 1 and 3. The sizes of the coarse grid and the BILU blocks are $16 \times 16 \times 16$ and $4 \times 4 \times 4$, respectively. Fig. 7 shows the although ILU requires large numbers of iterations to converge, its total computational time is less than that of BILU for all the cases we have studied.

To compare the efficiency of the iterative procedure including CF and the

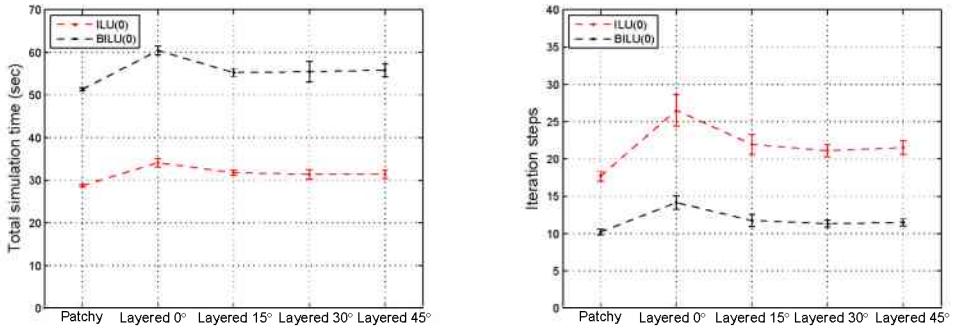

(a) (b)

Figure 7: The average and error bar plots of (a) total simulation time and (b) iteration steps for BILU and ILU comparison on layered and patchy permeability fields.

proposed modified CF (MCF) with ILU, permeability set 4 is considered. The fine and coarse grids contain $64 \times 64 \times 64$ and $8 \times 8 \times 8$ cells, respectively. Fig. 8 shows that MSFV-ILU is the best overall performedr;therefore, ILU is the most efficient local solver based on these findings.

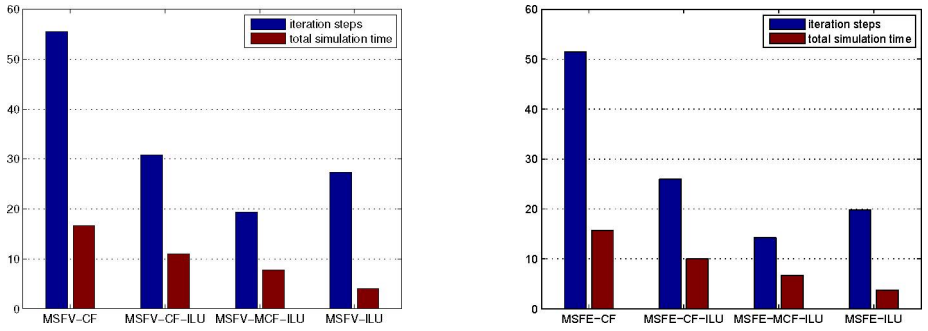

(a) (b)

Figure 8: Iteration steps and total simulation time (sec) for GMRES preconditioned by the MSFV (a) and MSFE (b) with CF, MCF, and ILU. Results are averaged over 20 realizations of patchy permeability field of set 4.

On the basis of our detailed investigation, we have found that MSFE with ILU leads to the best overall combination for solving the pressure equation of highly heterogenous systems. Next, our AMS method is compared with SAMG [28].

3.4 AMS vs. AMG

To investigate the efficiency of AMS compared with SAMG, which is widely used in the community, permeability set 5 (patchy field) is used. As shown in Table 1, this problem set consists of 32^3 fine cells. To increase the size of the domain, while keeping the same permeability statistics, a refinement procedure is employed, such that each grid cell is divided into 8 cells in each refinement step (split into two in each direction). Employing this refinement procedure, four grid sets are generated with 32^3, 64^3, 128^3 and 256^3 fine cells. For all the problem sizes, the coarsening factor is kept constant ($8 \times 8 \times 8$). The MSFE (with reduced boundary condition) and ILU are used as global and local solvers for AMS. The SAMG library is obtained from Fraunhofer Institute SCAI [28]. The scalability of AMS is illustrated in Fig. 9(a), where the computational times for different problem sizes are normalized with respect to the 32^3 case. The results are shown for both the setup and solution phases. Note that Fig. 9(b) shows that SAMG is slightly above the ideal line for the setup phase, which reflects its advanced coarsening algorithms.

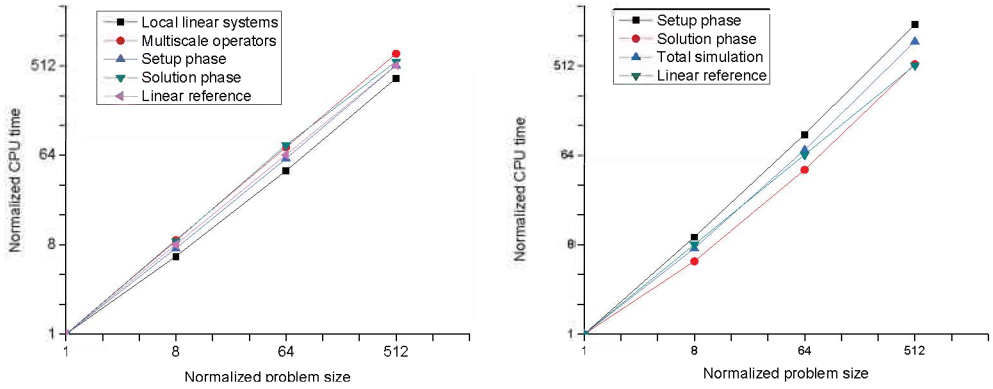

(a) AMS (b) SAMG

Figure 9: Scalability analysis of AMS and SAMG.

The performance of both AMS and SAMG is also tested and compared for permeability sets 1 and 3. The coarse grid consists of $16 \times 16 \times 16$ cells, and the same strategy for AMS, i.e., MSFE with reduced BC as global and ILU as local stages, is employed. Note that the permeability set 1 is a layered field, for which the Cartesian coarse grid is still used in the AMS coarse-scale solver. It is clear from Fig. 10 that SAMG outperforms AMS. The difference between the two is more pronounced for the layered field, which demonstrates that the coarsening strategy of AMS needs to be improved.

Also, Fig. 10 indicates that AMS and SAMG are comparable for large-scale systems. Having an AMS solver that is competitive with SAMG is important for the following reasons. First, it is clear that both AMS and SAMG have considerable setup times. For time-dependent problems, AMS is expected to benefit quite substantially from adaptive updating of the basis functions. Second, AMS is a mass-conservative iterative solver when the MSFV operator is employed the last step, and this is a critical requirement for solving time-dependent transport problems.

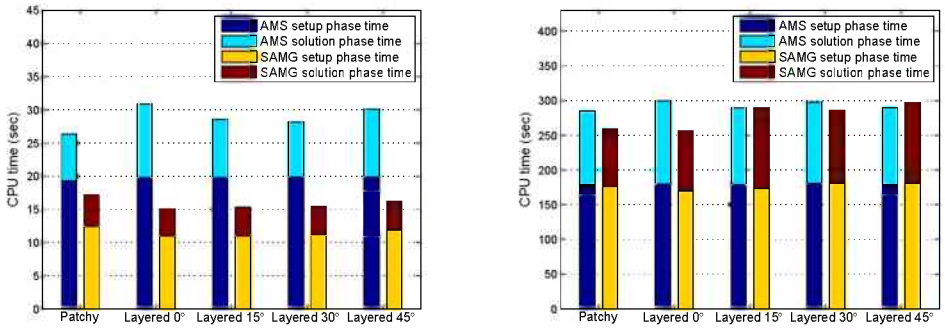

(a) Fine-scale grid is $128 \times 128 \times 128$ (b) Fine-scale size is $256 \times 256 \times 256$

Figure 10: Total, setup, and simulation times (sec) of AMS and SAMG as linear solvers for permeability sets 1 and 3. Results are averaged over 20 statistically-the-same realizations for each case.

4 Conclusions

In this work, a general Algebraic Multiscale Solver (AMS) for the pressure equation was developed. We analyzed the role of the Correction Function (CF) in the context of AMS, and we showed that the CF can be seen as an independent local stage. As a local preconditioner, CF helps to capture some of the high-frequency errors, especially in the source terms, and accelerates the overall convergence rate. However, - on average - the gain in convergence rate of using CF does not compensate for the additional computational cost. Simple preconditioners, such as ILU, are found to be more efficient than CF. Note that AMS with any combination of local- and global-stage solvers allows for the reconstruction of a conservative velocity field, if an MSFV stage is applied as the last step. Overall, the best AMS strategy is MSFE with reduced boundary conditions along with ILU. Our results indicate that the

performance of AMS is comparable to advanced algebraic multigrid solvers. Our results show that AMS is quite efficient, especially if it is used as a multiscale approximate (but conservative) solver for time-dependent subsurface flow problems.

Bibliography

[1] T. Hou and X. H. Wu. A multiscale finite element method for elliptic problems incomposite materials and porous media. *Journal of Computational Physics*, 134:169–189, 1997.

[2] Y. Efendiev, V. Ginting, T. Hou, and R. Ewing. Convergence of a nonconforming multiscale finite element method. *SIAM J. NUMER. ANAL.*, 37(3):888–910, 2000.

[3] J. Aarnes and T. Y. Hou. Multiscale domain decomposition methods for elliptic problems with high aspect ratios. *Acta Math. Appl.*, 18(1):63–76, 2002.

[4] T. Arbogast and S. L. Bryant. A two-scale numerical subgrid technique for waterflood simulations. *SPE Journal*, 7:446–457, 2002.

[5] Z. Chen and T. Hou. A mixed finite element method for elliptic problems with rapidly oscillating coefficients. *Mathematic Computation*, 72:541–576, 2003.

[6] P. Jenny, S. H. Lee, and H. A. Tchelepi. Multi-scale finite-volume method for elliptic problems in subsurface flow simulation. *Journal of Computational Physics*, 187:47–67, 2003.

[7] J. E. Aarnes. On the use of a mixed multiscale finite element method for greater flexibility and increased speed or improved accuracy in reservoir simulation. *Multiscale Modeling and Simulation*, 2(3):421–439, 2004.

[8] J. E. Aarnes, V. Kippe, and K. A. Lie. Mixed multiscale finite elements and streamline methods for reservoir simulation of large geomodels. *Advances in Water Resources*, 28(3):257–271, 2005.

[9] Y. Efendiev and T. Y. Hou. *Multiscale Finite Element Methods: Theory and Applications.* Springer, 2009.

[10] H. Hajibeygi and P. Jenny. Multiscale finite-volume method for parabolic problems arising from compressible multiphase flow in porous media. *Journal of Computational Physics*, 228:5129–5147, 2009.

[11] H. Zhou and H. A. Tchelepi. Operator-based multi-scale method for compressible flow. *SPE Journal*, 13:267–273, 2008.

[12] I. Lunati and P. Jenny. Multiscale finite-volume method for density-driven flow in porous media. *Computational Geosciences*, 12(3):337–350, 2008.

[13] C. Wolfsteiner, S. H. Lee, and H. A. Tchelepi. Well modeling in the multiscale finite volume method for subsurface flow simulation. *SIAM Multiscale Model. Simul.*, 5(3):900–917, 2006.

[14] P. Jenny and I. Lunati. Modeling complex wells with the multi-scale finite volume method. *Journal of Computational Physics*, 228:687–702, 2009.

[15] H. Hajibeygi, R. Deb, and P. Jenny. Multiscale finite volume method for non-conformal coarse grids arising from faulted porous media. *SPE 142205-MS, 21-23 Feb., The Woodlands, Texas*, 2011.

[16] H. Hajibeygi, D. Karvounis, and P. Jenny. A hierarchical fracture model for the iterative multiscale finite volume method. *Journal of Computational Physics*, 230(24):8729–8743, 2011.

[17] S. H. Lee, C. Wolfsteiner, and H. A. Tchelepi. A multiscale finite-volume method for multiphase flow in porous media: Black oil formulation of compressible, three phase flow with gravity. *Computational Geosciences*, 12:351–366, 2008.

[18] H. Hajibeygi and H. A. Tchelepi. Compositional multiscale finite-volume formulation. *SPE Journal*, 19(2), 2014.

[19] P. Jenny, S. H. Lee, and H. A. Tchelepi. Adaptive multiscale finite volume method for multi-phase flow and transport. *SIAM Multiscale Model. Simul.*, 3(1):50–64, 2004.

[20] P. Jenny, S. H. Lee, and H. A. Tchelepi. Adaptive fully implicit multi-scale finite-volume method for multi-phase flow and transport in heterogeneous porous media. *Journal of Computational Physics*, 217:627–641, 2006.

[21] H. Zhou, S. H. Lee, and H. A. Tchelepi. Multiscale finite-volume formulation for saturation equations. *SPE Journal*, 17(1):198–211, 2011.

[22] H. Hajibeygi and P. Jenny. Adaptive iterative multiscale finite volume method. *Journal of Computational Physics*, 230:628–643, 2011.

[23] M. A. Christie and M. J. Blunt. Tenth SPE comparative solution project: A comparison of upscaling techniques. *SPE Reservoir Evaluation and Engineering*, 4:308–317, 2001.

[24] V. Kippe, J. E. Aarnes, and K. A. Lie. A comparison of multiscale methods for elliptic problems in porous media flow. *Computational Geoscience*, 12(3):377–398, 2008.

[25] H. Hajibeygi, G. Bonfigli, M. A. Hesse, and P. Jenny. Iterative multiscale finite volume method. *Journal of Computational Physics*, 227:8604–8621, 2008.

[26] H. Zhou and H. A. Tchelepi. Two-stage algebraic multiscale linear solver for highly heterogeneous reservoir models. *SPE Journal*, SPE-141473-PA, 2012.

[27] E. Chow and M. A. Heroux. *BPKIT Reference Manual*. University of Minnesota Supercomputing Institute Technical Report UMSI 96/183, 1996.

[28] K. Stuben. *SAMG User's Manual*. Fraunhofer Institute SCAI, 2010.

[29] B. Smith, P. Bjorstad, and W. Gropp. *Domain Decomposition: Parallel Multilevel Methods for Elliptic Partial Differential Equations*. Cambridge University Press, 1996.

[30] J. Wallis and H. A. Tchelepi. Apparatus, method and system for improved reservoir simulation using an algebraic cascading class linear solver, U.S. Patent NO. 7684967, 2010.

[31] Y. Wang, H. Hajibeygi, and H. A. Tchelepi. Algebraic multiscale solver for flow in heterogeneous porous media. *Journal of Computational Physics*, 259:284–303, 2014.

[32] Y. Wang, H. Hajibeygi, and H. A. Tchelepi. Algebraic multiscale linear solver for heterogeneous elliptic problems. *Proceedings, 13th European Conference on the Mathematics of Oil Recovery*, 2012.

[33] N. Remy, A. Boucher, and J. Wu. *Applied geostatistics with SGeMS : a user's guide*. Cambridge University Press, New York, 2009.